EPR Characterization of Diamagnetic and Magnetic Organic Soft Materials Using Nitroxide Spin Probe Techniques

Rui Tamura,[a]* Katsuaki Suzuki,[a] Yoshiaki Uchida[b] and Yohei Noda[c]

Abstract: This review article summarizes the recent advance in the EPR studies on the molecular orientation and magnetic properties in the various rod-like liquid crystalline (LC) phases of the second-generation of organic nitroxide radical materials in the bulk state or in a surface-stabilized LC
10 cell, compared with the conventional EPR studies using classical organic nitroxide spin probes. Noteworthy is the first observation and characterization of a sort of spin glass-like ferromagnetic interactions ($\bar{J} > 0$) induced by weak magnetic fields in the various LC phases of the second-generation of organic nitroxide radical materials. This unique magnetic
15 property has been referred to as positive "magneto-LC effects". The utility of such novel LC nitroxide radical materials as the EPR spin probes is also presented.

X.1 Introduction

Electron paramagnetic resonance (EPR) spectroscopy using spin probes has been
20 widely recognized as a convenient and powerful means to obtain direct information on the molecular dynamics and microenvironment in various diamagnetic host materials. Particularly, the use of organic nitroxide radical compounds as spin probes has proved to be of great advantage to obtain the information concerning molecular local structure, mobility, micropolarity, acidity, and redox status in the
25 various condensed phases of host organic materials [1], because of the existence of the established analytical methodologies using EPR spectroscopy. For example, the EPR spectroscopy using nitroxide spin probes has been one of useful techniques for investigating the physical properties of organic liquid crystalline (LC) materials as the representative organic soft materials, such as the orientational order [2],
30 anisotropic interactions between non-LC solutes and LC solvents [3], fluctuation of director [4,5], anisotropy of molecular rotation [6,7], elastic behavior [8], and biaxiality [9]. In this context, a number of reports have been documented for the EPR studies using easily available non-LC nitroxide spin probes dissolved in diamagnetic host LC materials. In contrast, very few LC nitroxide spin probes were
35 developed, due most likely to the difficulty in the molecular design and synthesis which must satisfy the molecular linearity or planarity necessary for the existence of LC phases and the radical stabilization at the same time, although LC spin probes are anticipated to be more compatible with host LC materials than non-LC ones.

In this chapter, first we briefly survey both non-LC and LC nitroxide spin probes
40 which have been used for the EPR studies of diamagnetic host LC materials. Then the molecular alignment studies and the observation of unique magnetic interactions by EPR spectroscopy in the various LC phases of second-generation of rod-like

nitroxide radical materials, with and without using a surface-stabilized LC cell, are presented. From these studies, it would be well understood that EPR spectroscopy is an excellent tool for analyzing the magnetic properties of LC nitroxide radical soft materials at high temperatures, for which SQUID magnetization measurement is not
5 suited. In this article, we do not use the term 'spin-labelled LC materials', because the nitroxide radical unit in the second generation of LC nitroxide radical materials plays an important role in determining the molecular dielectric anisotropy as well as serving as the spin source.
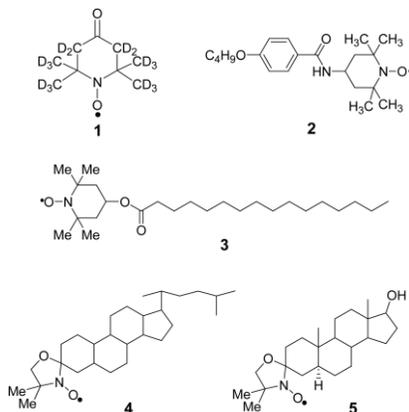

Figure 1 Molecular structures of typical non-LC nitroxide spin probes used in
10 diamagnetic host LC materials.

X.2 Non-LC nitroxide spin probes in diamagnetic LC hosts

As spin probes used in diamagnetic host LC materials, nitroxide radical materials such as **1–5** have been employed (Figure 1) [2-4, 10, 11].

The use of nitroxide spin probes provides three important parameters
15 characterizing EPR spectra; the g-value which is inversely proportional to the resonance magnetic field (H_0), the nitrogen hyperfine coupling constant (A), and the line-width (ΔH). For instance, an EPR spectrum of a nitroxide radical molecule dissolved in a diamagnetic host LC material is schematically shown in Figure 2. Since any motion of the nitroxide radical molecule is greatly influenced by the
20 molecular dynamics of the surrounding host molecules, the orientational order parameters (S) and rotational correlation times (τ_R), which characterize the molecular motion of the spin probe, are generally derived from these parameters according to the following theoretical equations [2].

$$S = \frac{(<a> - a)(g_x - g_y) - (<g> - g)(a_x - a_y)}{(a_z - a)(g_x - g_y) - (g_z - g)(a_x - a_y)} \tag{1}$$

25 where the subscripts x, y, and z refer to the principal axes of the **a**- and **g**-tensors determined in the rigid limit and <**a**> and <**g**> are their respective averages.

$$\tau_R = \left(\frac{2\sqrt{3}g_{iso}\beta_e}{\hbar b^2}\right)\left(\sqrt{\frac{I_0}{I_{+1}}} + \sqrt{\frac{I_0}{I_{-1}}} - 2\right)\Delta H_{pp0} \tag{2}$$

where β_e is the electron Bohr magneton, $\hbar$ is Plank's constant, I is the peak amplitude, and the subscripts +1, 0, -1 are nuclear quantum numbers for ^{14}N. ΔH_{pp0} is the peak-to-peak line-width of the centerline. The values of g_{iso} and b are calculated from the parameters for the immobilized spin probe:

$$g_{iso} = (g_x + g_y + g_z)/3 \tag{3}$$
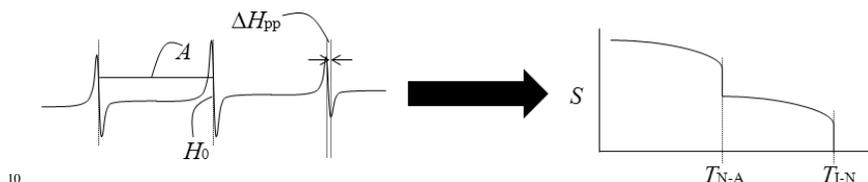
$$b = 2[a_z-(a_x+a_y)/2]/3 \tag{4}$$

Figure 2 Temperature (T) dependence of orientational order parameters (S) obtained from the EPR spectrum of a nitroxide radical molecule dissolved in a diamagnetic host LC material. T_{I-N} and T_{N-A} denote the Iso-N and N-SmA phase transition temperatures in the cooling process. Generally, S gradually increases with decreasing temperature and abruptly increases at the phase transition to result in a more ordered phase.

Evila et al. performed the EPR study on the order parameters and molecular dynamics using spin probe **2** in a reentrant nematic (R_N) liquid crystal mixture, 6OCB-8OCB [10]. The order parameter is shown as a function of temperature in the different phases (Figure 3). The ordering decreases slightly at the N-SmA and SmA-R_N transitions in the cooling run.
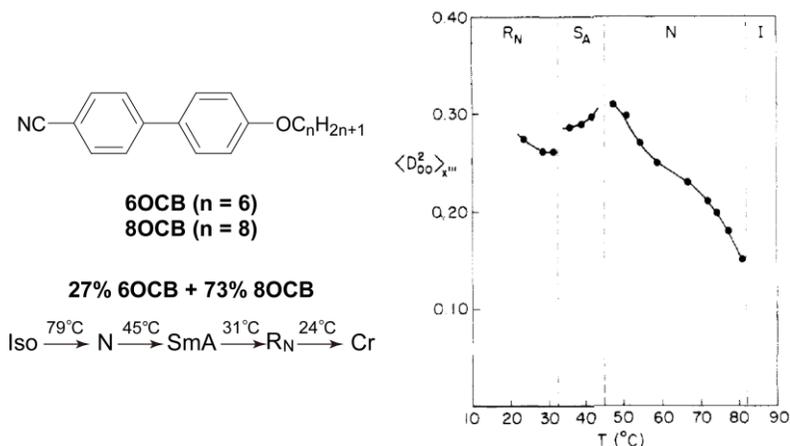

Figure 3 Molecular structures of **6OCB** and **8OCB**, and order parameter for spin probe **2** in a mixture of 6OCB and 8OCB. Ref. 10.

Although the EPR spin probe method is an excellent technique, non-LC spin probes may actually cause phase separation when they are mixed with the host LC materials [12]. In this case, the true molecular dynamics and microenvironment in the host LC phases cannot be evaluated. In fact, although this is another type of soft materials, the studies using the ionic liquid imidazolium nitroxide radical (±)-**6** as an EPR spin probe revealed that the τ_R value of (±)-**6** in the host ionic liquid **10** became much smaller than that simply estimated from the viscosity η of **10**, implying the existence of local structures in the host ionic liquid [13] (Figure 4). This behavior was not observed when typical neutral nitroxide spin probes such as TEMPO were employed with the same host **10** [13,14]. Accordingly, it is desirable to use an LC spin probe in a diamagnetic host LC material.
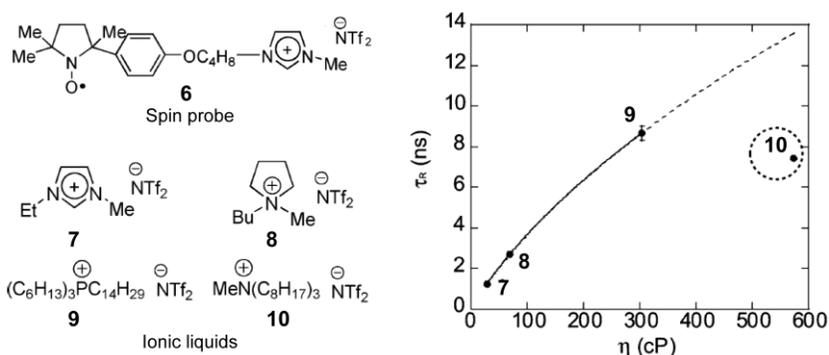

Figure 4. Molecular structures of the probe molecule and host ionic liquids, and rotational correlation time (τ_R) for (±)-**6** dissolved in the room temperature ionic liquids **7**-**10** plotted against the viscosity (η) of the solvents at 293K. Ref. 13.

X.3 LC nitroxide spin probes in diamagnetic LC hosts

Since two or more different materials showing the same LC phase are generally miscible, LC nitroxide radical materials could be used as appropriate spin probes for the diamagnetic host materials showing the same LC phase.

X.3.1 First-generation of rod-like LC nitroxide radical materials

Only a few rod-like LC nitroxide radical materials containing a DOXYL or TEMPO group within the terminal alkyl chain had been synthesized until 2003 (Figure 5) [15-20]. Dvolaitzky et al. synthesized the first LC nitroxide radicals **11**-**13** showing several smectic phases [15-17]. The EPR spectra of the spin probe **12** dissolved in diamagnetic host LC materials changed at LC-to-LC phase transition [15]. However, as long as the LC nitroxide radical materials illustrated in Figure 5 were employed as spin probes, it is difficult to determine the exact direction of molecular alignment of the spin probes and host materials to the applied magnetic field, due to the free rotation of the nitroxide radical unit inside the molecule and the possible phase separation (see Section X.2).
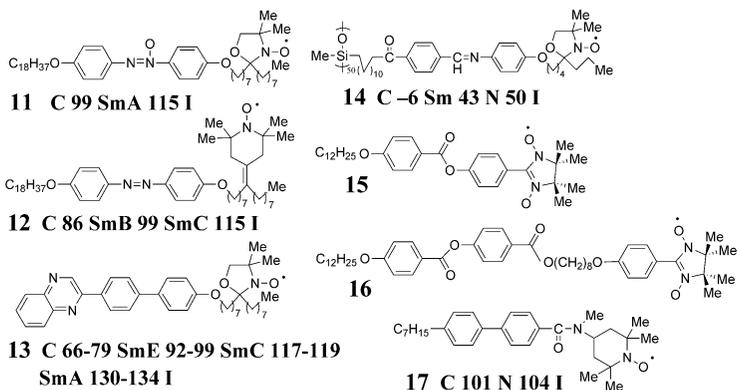
11   C 99 SmA 115 I

12 C 86 SmB 99 SmC 115 I

**13 C 66-79 SmE 92-99 SmC 117-119
SmA 130-134 I**

14 C –6 Sm 43 N 50 I

15

16

17 C 101 N 104 I

Figure 5 Molecular structures of the first-generation of rod-like LC nitroxide radical materials.

X.3.2 Second-generation of rod-like LC nitroxide radical materials

5 In 2004, the design and synthesis of a new type of chiral LC nitroxide radical materials **18** (Figure 6), which could satisfy the following four requirements and showed chiral (or achiral) nematic [N* (N)] and/or smectic C [SmC* (SmC)] phases at wide temperature range below 90°C, were reported by the present authors [21-24].
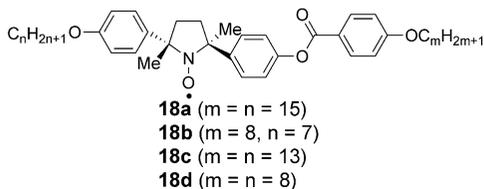
18a (m = n = 15)
18b (m = 8, n = 7)
18c (m = n = 13)
18d (m = n = 8)

Figure 6 Molecular structure of the second-generation of rod-like LC nitroxide
10 radical materials **18** with a radical unit in the core portion.

(1) *Spin source*: A nitroxyl group with a large electric dipole moment (ca. 3 Debye) and known principal g-values (g_{xx}, g_{yy}, g_{zz}) should be the best spin source, because i) the dipole moment is large enough for the source of the spontaneous
15   polarization (Ps) and ii) the principal g-values are useful to determine the direction of molecular alignment in the LC phase by EPR spectroscopy (Figure 7).

(2) *High thermal stability*: A molecule with 2,2,5,5-tetraalkyl-substituted pyrrolidine-1-oxy (PROXYL) unit is stable enough for repeated heating and
20   cooling cycles below 150 °C in the air.

(3) *Molecular structure*: (a) To avoid the free rotation of the nitroxide radical unit inside the molecule so as to maximize the $\Delta\chi_{para}$ and $\Delta\varepsilon$, a geometrically fixed chiral cyclic nitroxide radical unit should be incorporated into the rigid core of LC molecules. (b) To obtain a slightly zigzag molecular structure and a
25   negative $\Delta\varepsilon$ advantageous for the appearance of a ferroelectric SmC* phase, a *trans*-2,5-dimethyl-2,5-diphenylpyrrolidine-1-oxy   (PROXYL)   skeleton   in

which the electric dipole moment orients to the molecular short axis is the best choice (Figure 7).

(4) *Chirality*: Since both chiral and achiral LC materials are required for comparison of their optical and magnetic properties in the various LC phases, the molecules should be chiral and both enantiomerically enriched and racemic samples need to be available.
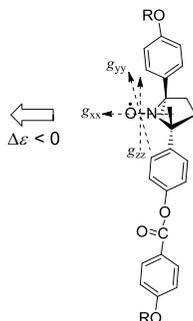

Figure 7 Principal *g*-values and dielectric anisotropy in the nitroxide radical **18**.

Chumakova *et al.* reported the ordering of the LC spin probes (*S*,*S*)-**18a** (m=n=15) and (±)-**18a** dissolved in the magnetically aligned nematic matrix of achiral *N*-(4-methoxybenzylidene)-4-butylaniline (MBBA) in detail [25]. This work demonstrated that the change of the orientation distribution of **18a** reflects only the structural change of the host LC material, irrespective of the chirality of spin probes (Figure 8), and that the LC nitroxide radical molecules are built in the diamagnetic LC material more successfully than non-LC TEMPO radical.
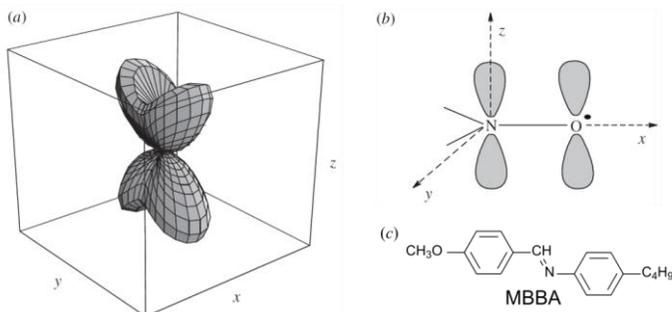
Figure 8 (a) Orientation distribution function of the nitroxide radical **18a** in aligned MBBA; (b) directions of the main axes of *g*-tensor in molecules of nitroxide radicals; (c) molecular structure of MBBA. Ref. 25.

X.4 Magnetic properties of second-generation of rod-like LC nitroxide radical materials

When the concentration of a nitroxide spin probe in a diamagnetic host material is low enough, the conventional methodologies to estimate the orientational order of the spin probe by using ΔH and A values can be employed. In contrast, when the

nitroxide radical material is not diluted by the diamagnetic host material, the radical spin-spin interactions prevail over the hyperfine coupling interactions between electron and nuclear spins, resulting in the ΔH increase and the loss of hyperfine coupling structure [26] (Figure 9). In this case, orientational order and

5 intermolecular magnetic interactions can be evaluated by analysing the g-values and ΔH change, respectively.

In this section, the following four current findings by the present authors are described: (1) The principal g-values ($g_{//}$ and $g_{\perp}$) and molecular orientation of the LC nitroxide radical molecule **18b** (m=8, n=7) confined in a surface-stabilized LC

10 cell were determined by EPR spectroscopy [27]. (2) The magnetic-field-induced molecular orientation in the bulk nematic and SmC phases of ($\pm$)-**18c** (m=n=13) was determined by EPR spectroscopy [28]. (3) The unique spin glass-like intermolecular ferromagnetic interactions ($\bar{J} > 0$), which were referred to as positive "magneto-LC effects", were found to generate in the various LC phases of **18** in weak magnetic

15 fields by EPR spectroscopy and SQUID magnetization measurement [29,30]. (4) The existence of anisotropy in the intermolecular ferromagnetic interactions responsible for the positive magneto-LC effects was proved by the measurement of the electric field dependence of molecular orientation and magnetic interactions in a surface-stabilized ferroelectric LC cell of (S,S)-**18c** showing an SmC* phase.
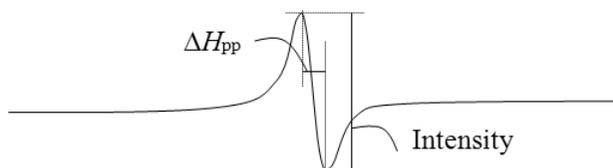
20

Figure 9 A typical EPR differential curve measured for an LC phase of nitroxide radical materials **18**. Peak-to-peak line width (ΔH_{pp}), intensity, and resonant magnetic field of the spectrum reflect the static and dynamic properties of the LC phase of **18**.

25

X.4.1 Molecular orientation in the N and N* phases confined in a surface-stabilized LC cell

It is well-known that the orientation of LC molecules can be controlled by using a surface-stabilized LC cell. However, until 2005 there was no report on the study of

30 the orientation of LC molecules in a surface-stabilized LC cell by EPR spectroscopy. The present authors reported for the first time the molecular orientation in the N and N* phase of **18b** confined in surface-stabilized LC cells (Figure 10) [27].
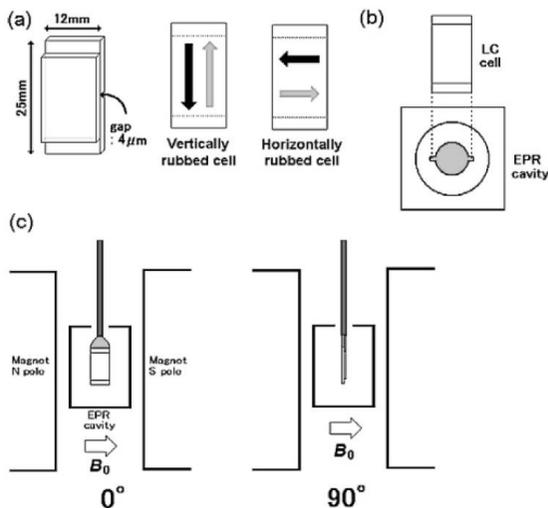
Figure 10 (a) LC cell appearance (left) and vertically and horizontally rubbed cells (middle and right). The black and gray allows indicate the rubbing direction of top and bottom planes, respectively. (b) Top view of the EPR cavity, which was designed for the insertion and rotation of the LC cells. (c) Definition of the rotation angles of the LC cell to the applied magnetic field. Reprinted with permission from ref. 27. Copyright 2012 American chemical Society.

First, the angular dependence of g-value for the N and N* phases of ($\pm$)-**18b** and (S,S)-**18b**, respectively, was measured by EPR spectroscopy. For the N phase of ($\pm$)-**18b**, the angular profile of the vertically rubbed cell was flat, while that of horizontally rubbed cell oscillated significantly (Figure 11a). In contrast, for the N* and crystalline phases of (S,S)-**18b**, the angle profiles of both rubbed cells were almost identical (Figure 11b, c). These experimental results can be explained by the orientation models shown in Figure 12. In the LC phases, the rotation axis fluctuates from the director (the average direction of the molecular long axis). To take this fluctuation into account, $g_{//}$ was defined as the ensemble g-value observed when the magnetic field is applied parallel to the director and $g_{\perp}$ as the ensemble g-value observed when the magnetic field is applied orthogonally to the director.
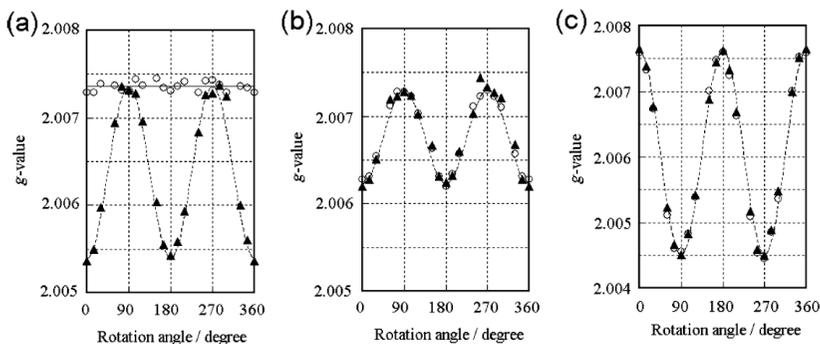

Figure 11 Angular dependence of the g-value for (a) the N phase of ($\pm$)-**18b**, (b) the N* phase of (S,S)-**18b**, and (c) the crystalline phase of (S,S)-**18b**. White circles ($\circ$) and black triangles ($\blacktriangle$) indicate the g-values for the vertically and horizontally rubbed cells, respectively. Reprinted with permission from ref. 27. Copyright 2012 American

chemical Society.

The orientation model for the N phase of (±)-**18b** indicates that the LC molecule rotates around the long axis of the molecule, which is aligned with the rubbing direction on the cell surface, and that the direction of the long axis is uniform throughout the cell (Figure 12a). Since the angle between the magnetic field direction and the long axis of the molecule varies between 0 and 90° for the horizontally rubbed cell (▲), $g_{//}$ or $g_{\perp}$ is alternately observed. For the vertically rubbed cell (○), $g_{\perp}$ is observed constantly since the magnetic field is always orthogonal to the director.

The orientation model for the N* phase of (*S*,*S*)-**18b** indicates that the LC molecule rotates around the long axis of the molecule, which aligns with the rubbing direction on the cell plane, and that the long axis between the two cell planes rotates to form a helical superstructure (Figure 12b). The agreement between the angular profiles of horizontally and vertically rubbed cells is due to this helical superstructure.

To determine the $g_{//}$ and $g_{\perp}$ values, the temperature dependence of the g-value was measured for the N phase of (±)-**18b** confined in a horizontally rubbed cell at the angles of 0 and 90° (Figure 13a). The temperature dependence of the g-value followed the Haller equation [31,32]:

$$g_{//}(T) = g_{//}(1 - T/T^*)^{\beta} \tag{5}$$

$$g_{\perp}(T) = g_{\perp}(1 - T/T^*)^{\beta} \tag{6}$$

where T is the temperature (K), T^* is the transition temperature (K) between the N and isotropic phases, and β is the exponent parameter.

The solid curve in Figure 13a was calculated by assigning $g_{//}$ = 2.00456, $g_{\perp}$ = 2.00754, T^* = 376K, and β = 0.136 to give the best fit with the experimental result. Furthermore, the same temperature profile of the order parameters S was obtained according to the following equations (Figure 13b).

$$S(T) = (g_{//}(T) - g_{iso})/(g_{//}\text{-}g_{iso}) \tag{7}$$

$$S(T) = (g_{\perp}(T) - g_{iso})/(g_{\perp}\text{-}g_{iso}) \tag{8}$$

Another approach was carried out to obtain $g_{//}$ and $g_{\perp}$ by conducting a coordinate transformation of a set of principal g-values of a similar nitroxide molecule into the molecular long axis frame [27]. These calculated g values ($g_{//}$ = 2.00477, $g_{\perp}$ = 2.00744) are in good agreement with the g values obtained by the Haller fitting of the temperature-dependence experiment.

Thus, the method described in this work has proved to be effective for the determination of the orientation and order parameters S of LC molecules based on the principal g-values ($g_{//}$ and $g_{\perp}$).

In a similar manner, the molecular orientation in the SmC and SmC* phases of (±)-**18c** and (*S*,*S*)-**18c**, respectively, was determined by using a surface-stabilized LC cell [33].
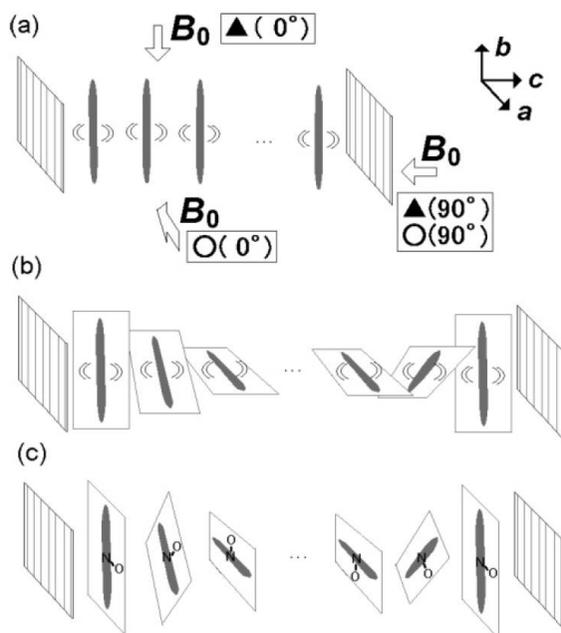
Figure 12 Orientation models of LC molecules in an LC cell for (a) the N phase of (±)-**18b**, (b) the N* phase of (*S,S*)-**18b**, and (c) the crystalline phase of (*S,S*)-**18b**. The square planes on both sides indicate the LC cell surface, and the stripes on the cell surface indicate the rubbing direction. The gray rod indicates an LC molecule. The double arcs drawn on both sides of the gray rod indicate the rotator motion of the LC molecules. Reprinted with permission from ref. 27. Copyright 2012 American chemical Society.
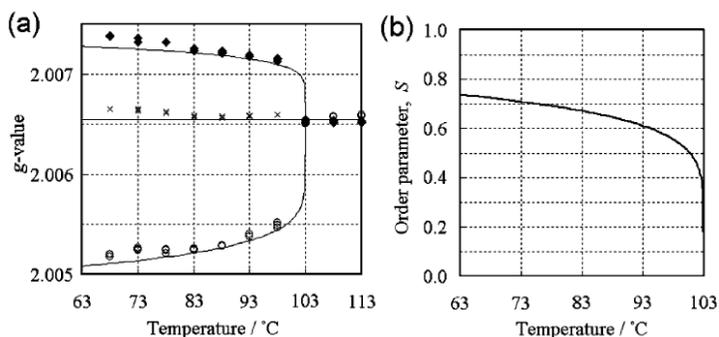

Figure 13. Temperature dependence of the g-value of (±)-**18b** in a horizontally rubbed cell. The white circles or black diamonds indicate g-values observed when the angle between the magnetic field and the director of LC molecule is 0° ($g_{//}$) or 90° ($g_{\perp}$), respectively. The cross signs (×) indicate g_{ave} [($g_{//}$ + 2 $g_{\perp}$)/3]. The solid curve is calculated by the Haller equation. (b) Calculated curve of the order parameter, S. Reprinted with permission from ref. 27. Copyright 2012 American chemical Society.

X.4.2 Molecular orientation in the bulk N and SmC phases

LC nitroxide radical materials **18** with low viscosity, low phase transition temperature, and principal g-values of the nitroxide moiety are considered to be a

good candidate for the studies on the $\Delta\chi$–controlled molecular orientation by weak magnetic fields. Therefore, we determined whether the magnetic-field-induced molecular alignment in the LC phases of **18** was dominated by the $\Delta\chi_{para}$ or $\Delta\chi_{dia}$, based on the quantitative evaluation of the $\Delta\chi_{para}$ and $\Delta\chi_{dia}$ values of **18**.

First, the temperature-dependent $\Delta\chi_{para}$ value of **18c** was calculated to be -1.7 x 10^{-6} emu mol^{-1} at 300 K from the g-value obtained by EPR spectroscopy, while the temperature-independent $\Delta\chi_{dia}$ value was calculated to be $+6.5$ x 10^{-5} emu mol^{-1} from the experimental molar magnetic susceptibility (χ_M) of ($\pm$)-**18c** measured on a SQUID magnetometer [28]. Thus, $|\Delta\chi_{dia}|$ turned out to be 30 times larger than $|\Delta\chi_{para}|$; the molecular alignment of **18c** by magnetic fields is definitely $\Delta\chi_{dia}$-controlled, if the orientation restriction due to the surface is weak.

To identify the direction of molecular alignment in the bulk LC state under a weak magnetic field, the temperature dependence of the experimental g-value (g_{exp}) of ($\pm$)-**18c** was measured at a magnetic field of 0.33 T by EPR spectroscopy (Figure 14) [28]. During the heating process, the g_{exp} of ($\pm$)-**18c** was constant at around 2.0065 in the crystalline state, then increased at the crystal-to-SmC phase transition, became constant at around 2.0068 in the SmC phase, then decreased abruptly to 2.0058 at the SmC-to-N phase transition, and finally returned to the level ($\sim$ 2.0065) of the crystalline state in the isotropic phase. During the cooling process, the g_{exp} of ($\pm$)-**18c** was constant at around 2.0065 in the isotropic phase, then decreased at the Iso-to-N phase transition, became constant at around 2.0055 in the N phase, then increased to 2.0063 at the N-to-SmC phase transition, and finally increased to 2.0067 in the crystalline state.
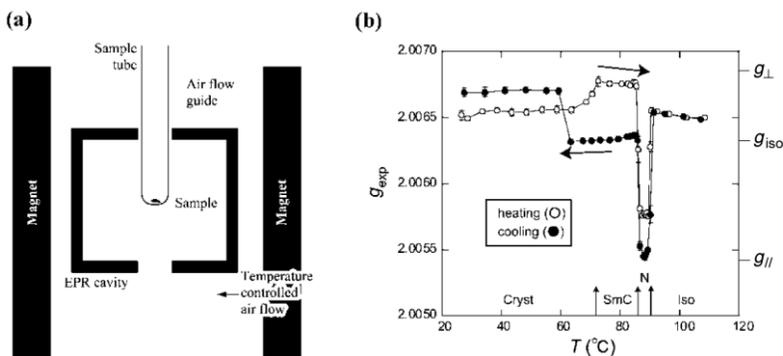

Figure 14 EPR spectroscopy of ($\pm$)-**18c** (m=n=13). (a) Experimental setup and (b) temperature dependence of the g-value measured through the first heating (white circles) and cooling (black circles) processes. Ref. 28

From these results and the calculated principal g-values (g_{iso}=2.00632, $g_{//}$=2.00540, $g_{\perp}$=2.00678) of **18c**, it was concluded that i) in the N phase the majority of molecules align their long axis along the applied magnetic field of 0.33 T (Figure 15a), whereas in the SmC phase during the heating process the molecular short axis is fairly parallel to the field (Figure 15b), most likely due to the viscous layer structure and the natural homeotropic anchoring effect by quartz surface, and ii) that the molecular alignment in each LC phase is influenced by that in the preceding LC phase, although the molecular orientation modes are quite different between the N and SmC phases.
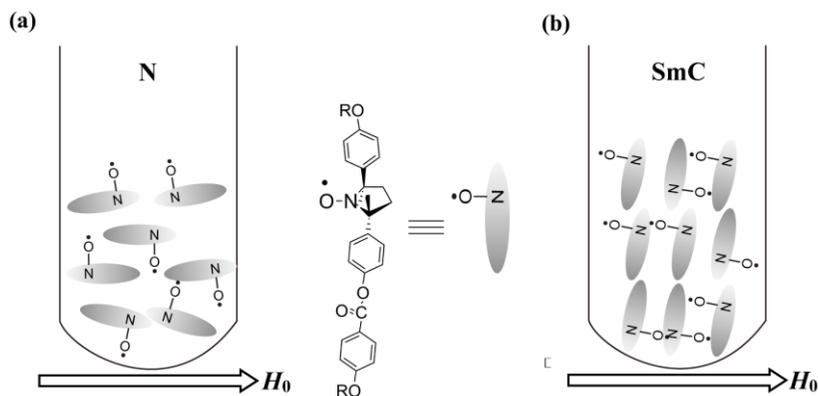
Figure 15 Molecular alignment in the LC phases of (±)-**18c** under a weak magnetic field (0.33 T). (a) N phase during both heating and cooling processes and (b) SmC phase during the heating process.

X.4.4 Intermolecular magnetic interactions

X.4.4.1 Magneto-LC effects observed in the bulk LC state

To investigate whether there are appreciable intermolecular magnetic interactions in the LC phases of nitroxide radical materials **18** with negative dielectric anisotropy ($\Delta\varepsilon < 0$), the temperature dependence of EPR spectra was measured for **18c** (m=n=13) and **18d** (m=n=8) [29]. EPR spectroscopy is the much better means than SQUID magnetization measurement to measure the temperature dependence of the χ_{para} for LC nitroxide radical materials at high temperatures. This is due to the following four reasons: (i) The χ_{para} can be derived from the Bloch equation by using the parameters obtained from the EPR differential curves, such as maximum peak height (I'_m and $-I'_m$), g-value (g) , and peak-to-peak line width (ΔH_{pp}).

$$\chi_{para} = \frac{2\mu_B g I'_m \Delta H_{pp}^2}{\sqrt{3} h \nu H_1}$$

(9)

where μ_B is the Bohr magneton, h is Planck's constant, ν is the frequency of the absorbed electromagnetic wave, and H_1 is the amplitude of the oscillating magnetic field. Accordingly, the temperature dependence of relative paramagnetic susceptibility (χ_{rel}), which is defined as

$$\chi_{rel} = \frac{\chi_{para}}{\chi_0}$$

(10)

where χ_0 is the standard paramagnetic susceptibility, e.g., at 30°C in the heating run can be actually used (Figure 16). (ii) Treatment of the χ_{dia} term is totally unnecessary. (iii) The experimental error is very small even at high temperatures. (iv) The analysis of microscopic magnetic interactions such as spin-spin dipole and exchange interactions is also feasible.

First, the temperature dependence of χ_{rel} for (±)-**18c** and (S,S)-**18c** (88% *ee*), and (±)-**18d** (96% *ee*) and (S,S)-**18d** was studied [29]. All of these four samples showed

a considerable net χ_{rel} increase at each Cr-to-LC phase transition in the heating run, similarly to the case of SQUID magnetometry (Figure 16) [29,30]. In combination with the experimental results on the magnetic field dependence of magnetization measured by SQUID magnetometry for these four LC phases of **18c** and **18d**, it was
5 concluded that a sort of spin glass-like inhomogeneous ferromagnetic interactions induced by weak magnetic fields should operate in the various LC phases. This unique magnetic property, which was referred to as positive "magneto-LC effects" (average spin-spin interaction constant, $\bar{J} > 0$) [34], proved to have nothing to do with the molecular reorientation effect arising from the simple molecular magnetic
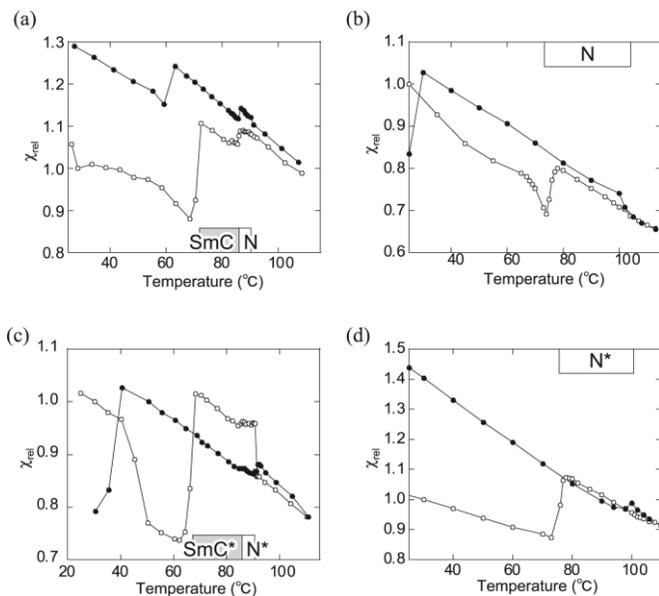10 anisotropy ($\Delta\chi$) [29].

Figure 16 Temperature dependence of relative paramagnetic susceptibility (χ_{rel}) for (a) (±)-**18c**, (b) (±)-**18d**, (c) (*S,S*)-**18c** (88% *ee*), and (d) (*S,S*)-**18d** (96% *ee*) at a
15 magnetic field of 0.33 T. Open and filled circles represent the first heating and cooling runs, respectively. The LC temperatures shown in a box refer to the first heating process. Reprinted with permission from ref. 29. Copyright 2012 American chemical Society.

20 To gain an insight into the origin of the positive magneto-LC effects operating in the LC phases of **18c** and **18d**, the temperature dependence of ΔH_{pp} and *g*-value was compared with that of χ_{rel} for these four samples (Figure 17) [29]. This is because (1) the change in ΔH_{pp} reflects the following two competing factors, (a) spin-spin dipole interaction (the stronger the interaction is, the more the ΔH_{pp} increase is) and
25 (b) spin-spin exchange interaction (the stronger the interaction is, the more the ΔH_{pp} decrease is) and (2) the change in *g*-value corresponds to that in the molecular orientation in the magnetic field. Consequently, the χ_{rel} increase was accompanied by the ΔH_{pp} increase and the *g*-value decrease at each crystal-to-LC phase transition for (*S,S*)-**18c**, (±)-**18d** and (*S,S*)-**18d** in the heating run (Figure 17f-h), indicating the
30 generation of the most stable ferromagnetic head-to-tail spin-spin dipole interactions

in the LC phases, irrespective of the g-value change (Figure 18). On the other hand, although the ΔH_{pp} decrease was observed with the χ_{rel} increase at the crystal-to-SmC phase transition for (±)-**18c** in the heating run (Figure 17e), this phenomenon can be interpreted in terms of generation of the large spin-spin exchange interactions,
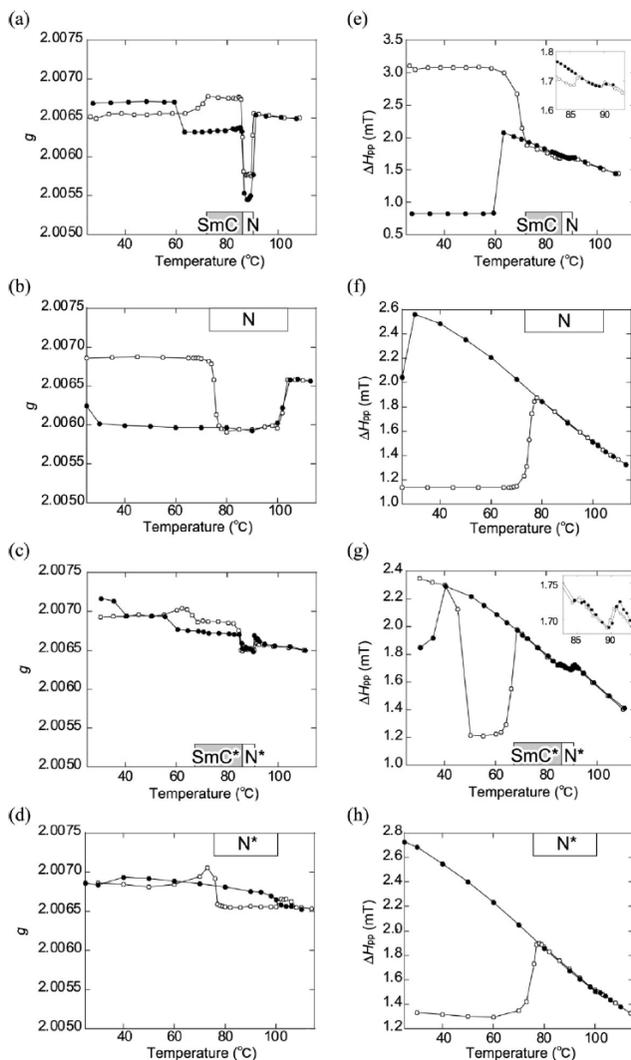5 together with ferromagnetic head-to-tail spin-spin dipole interactions.

Figure 17 Temperature (T) dependences of g-value and ΔH_{pp} for **18c** and **18d** by EPR spectroscopy. At a field of 0.33 T in a temperature range of 25 to 115 °C. (a and e) (±)-
10 **18c**; (b and f) (±)-**18d**; (c and g) (S,S)- **18c** (88% ee),; (d and h) (S,S)- **18d** (96% ee). Open and filled circles represent the first heating and cooling runs, respectively. The insets in panels e and g indicate the magnification of the ΔH_{pp} Vs T plots in the temperature range of 83 to 93 °C. The LC temperatures shown in a box, which were determined by DSC analysis at a scanning rate of 5 °C min⁻¹, refer to the first heating process.
15 Reprinted with permission from ref. 29. Copyright 2012 American chemical Society.
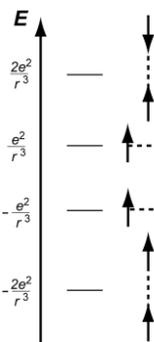
E

$$\frac{2e^2}{r^3}$$

$$\frac{e^2}{r^3}$$

$$-\frac{e^2}{r^3}$$

$$-\frac{2e^2}{r^3}$$

Figure 18. Relative stability of possible four spin-spin dipole interactions between two spins.
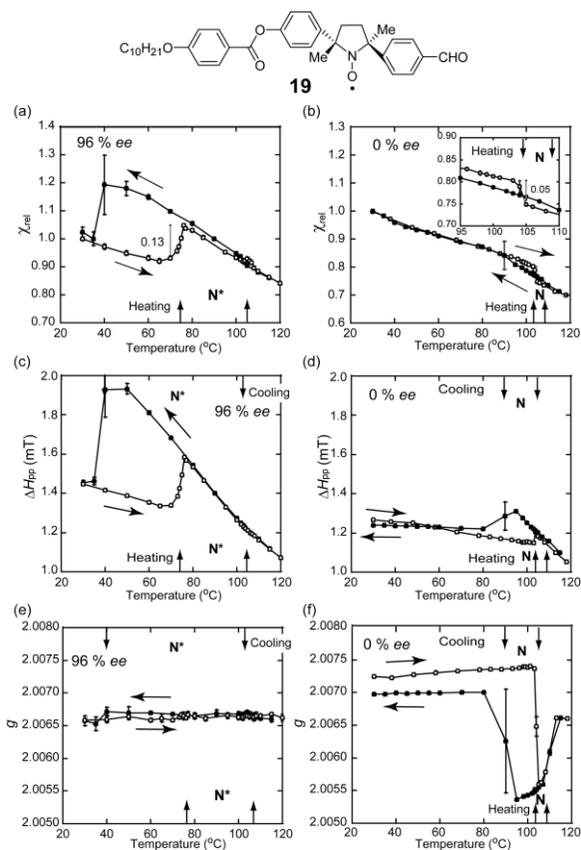
19

Figure 19. Temperature dependence of relative paramagnetic susceptibility (χ_{rel}), ΔHpp, and g-values for **19** at a magnetic field of 0.33 T. (a, c, and e) (S,S)-**19** (96% ee) and (b, d, and f) (±)-**19**. Open and filled circles represent the first heating and cooling runs, respectively. The LC temperatures determined by DSC analysis in the heating run are shown in the lower side inside panels. Ref. 34.

To clarify the relationship between the sign ($\overline{J} > 0$ or $\overline{J} < 0$) and magnitude of magneto-LC effects and the sign ($\Delta\varepsilon < 0$ or $\Delta\varepsilon > 0$) of dielectric anisotropy, a new LC material **19** with positive dielectric anisotropy ($\Delta\varepsilon < 0$) was synthesized.
5 Interestingly, strong positive magneto-LC effects ($\overline{J} > 0$) operated in the N* phase of (*S,S*)-**19** (96% *ee*), whereas weak negative magneto-LC effects ($\overline{J} < 0$) were observed in the N phase of (±)-**19** (Figure 19) [34].

To gain an insight into the origin of the negative or positive magneto-LC effects ($\overline{J} < 0$ or $\overline{J} > 0$) operating in the N phase of (±)-**19** or in the N* phase of (*S,S*)-**19**,
10 the temperature dependence of ΔH_{pp} and g values was compared with that of χ_{rel} for these samples. In the case of (±)-**19**, a slight increase in ΔH_{pp} occurred in concert with the slight decrease in χ_{rel} at the Cr-to-N transition in the heating run, irrespective of the *g*-value change, indicating the increase of spin-spin dipole interactions in the N phase of (±)-**19**. Accordingly, it is quite natural to consider that
15 the negative magneto-LC effects operating in the N phase of (±)-**19** originate from the generation of antiferromagnetic interactions due to the local SOMO-SOMO overlapping in the strong *RS* magnetic dipolar interaction in which the side-by-side spin-spin dipole interactions should dominate (Figure 20b).

In contrast, at the Cr-to-N* transition of (*S,S*)-**19**, both ΔH_{pp} and χ_{rel} distinctly
20 increased without no molecular reorientation in the magnetic field, reflecting the dominant generation of the energetically favoured ferromagnetic head-to-tail spin-spin dipole interactions, as observed in the N* phase of (*S,S*)-**18d** (Figure 20a).
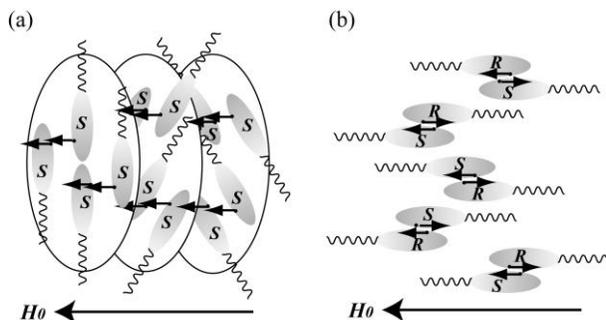

Figure 20 Spin-spin dipole interactions in LC phases. (a) N* phase of (2*S*,5*S*)-**19** and (b) N phase of (±)-**19**. Ref.34.

25

X.4.4.2 Anisotropic positive magneto-LC effects observed in a surface-stabilized ferroelectric LC cell.

To prove the existence of spin easy axis or the anisotropy of intermolecular ferromagnetic interactions responsible for the positive magneto-LC effects observed
30 in the LC phases of nitroxide radical materials **18** described in Section X.4.4.1, the electric field dependences of molecular orientation and magneto-LC effects were measured in a surface-stabilized ferroelectric LC cell of (*S,S*)-**18c** showing an SmC* phase by EPR spectroscopy (Suzuki, K., Uchida, Y., Tamura, R. et al., manuscript submitted for publication).
35 The sample of (*S,S*)-**18c** of 65% *ee* was introduced by capillary action into the lower tip (4 mm x 4 mm area) of a handmade 4 μm-thick sandwich cell (50 mm x 5

mm) in which the inner surfaces of two glass substrates with indium tin oxide (ITO) electrodes were coated with polyimide polymer (Figure 21). The magnetic field was applied perpendicular to the electric field and parallel to the rubbing direction (Figure 22d).
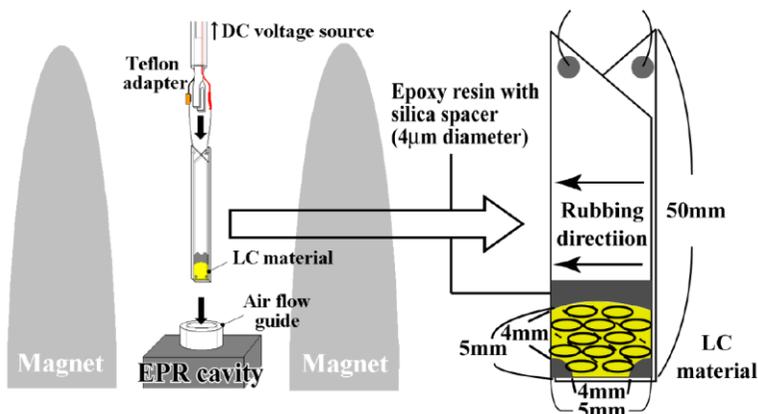

Figure 21. Experimental setup to monitor variable-temperature EPR spectra of (*S,S*)-18c using a long sandwich cell.
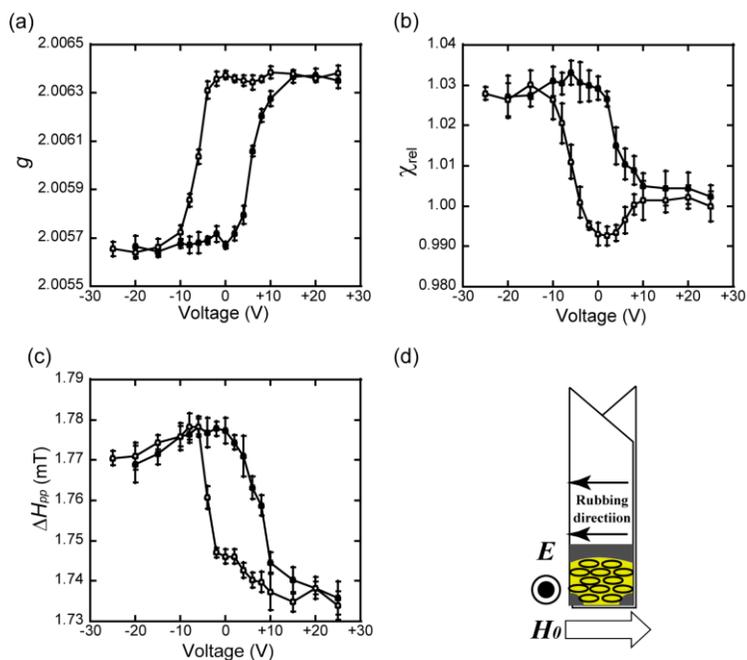
Figure 22. Electric field dependence of (a) g, (b) χ_{rel}, and (c) ΔH_{pp} values in a thin rubbed sandwich cell of the ferroelectric SmC* phase of (*S,S*)-18c at 75°C by EPR spectroscopy. (d) The magnetic field was applied perpendicular to the electric field and parallel to the rubbing direction. Open and filled circles represent the application of electric fields from +25V to −25V and from −25V to +25V, respectively.

First, the existence of ferroelectric bistable state was confirmed in an EPR cavity at a magnetic field of 0.33T by evaluating the electric field dependence of g value (Figure 22a). The experimental g value (g_{exp}) of (S,S)-**18c** exhibited a hysteresis loop between +25 V and −25 V. Since the $g_{//}$ and $g_\perp$ values of **18c** were previously determined to be 2.0054 and 2.0068, respectively [28], the g_{exp} value (2.0057) at −25V seems to reflect a large contribution of $g_{//}$, suggesting that the molecular long axis of (S,S)-**18c** aligns almost parallel to the magnetic field (Figure 23a). Reduction of the electric field to 0 V did not change the molecular orientation owing to its sufficient ferroelectric memory effect. Meanwhile, the g_{exp} value (2.0063) at +25V indicates that the molecular long axis of (S,S)-**18c** is fairly tilted from the direction of the magnetic field (Figure 23b). Thus, (S,S)-**18c** has proved to take a surface stabilized ferroelectric bistable state between +25 V and −25 V.

The electric field dependence of χ_{rel} for (S,S)-**18c** showed a hysteresis loop between +25 V and −25 V (Figure 22b). Since the molecular long axis is parallel to the magnetic field at −25 V, the spin easy axis in the ferroelectric LC phase of (S,S)-**18c** has proved to lie along the molecular long axis.

To gain an insight into the origin of the anisotropic positive magneto-LC effects ($\overline{J} > 0$) operating in the ferroelectric LC phase of (S,S)-**18c**, the electric field dependence of ΔH_{pp} was compared with that of χ_{rel} for (S,S)-**18c** (Figure 22b,c). If the χ_{rel} change results from the spin-spin exchange interaction, the experimental ΔH_{pp} would decrease with increasing χ_{rel}. However, the observed ΔH_{pp} increased or decreased with increasing or decreasing χ_{rel}, respectively. This result suggests that the observed electric field dependence of χ_{rel} primarily should arise from the change in the spin-spin dipole interaction. There are two types of spin-spin dipole interactions; one is a head-to-tail type and the other is a side-by-side type (Figure 18). Since the ferromagnetic head-to-tail dipole interaction is energetically favored over the antiferromagnetic side-by-side dipole interaction, it is easily envisaged that two interacting spins should take different head-to-tail configurations at −25 V and +25 V in the ferroelectric SmC* phase of (S,S)-**18c** (Figure 23); the spin-spin dipole interaction at −25 V was stronger than that at +25 V, leading to the higher χ_{rel} value at −25 V than that at +25 V (Figure 22b,c). Thus, the existence of spin easy axis in the ferroelectric SmC* phase of (S,S)-**18c** has been proved; strong spin-spin dipole interactions operated when the magnetic field was applied parallel to the molecular long axis.

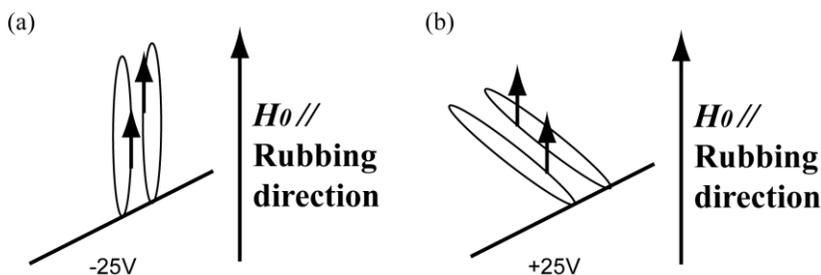

Figure 23. Spin-spin interactions between localized spins in the ferroelectric SmC* phase. The molecular long axis is (a) almost parallel to the magnetic field at −25V and (b) tilted from the direction of the magnetic field at +25V.

X.5 Conclusions

The recent advance in our EPR studies concerning the following molecular orientation and magnetic properties with respect to the various rod-like LC phases of the second-generation of organic nitroxide radical materials **18** and **19** in the bulk state or in a surface-stabilized LC cell is briefly reviewed; (1) the determination of the principal g-values ($g_{//}$ and $g_{\perp}$) of **18** and the molecular orientation in the N phase of **18** confined in a surface-stabilized LC cell by EPR spectroscopy, (2) the determination of the magnetic-field-induced molecular orientation in the bulk nematic and SmC phases of **18** by EPR spectroscopy, (3) the first observation by EPR spectroscopy of the positive magneto-LC effects ($\bar{J} > 0$) induced by weak magnetic fields in both chiral and achiral rod-like LC phases of **18** with negative dielectric anisotropy ($\Delta\varepsilon < 0$), together with the positive and negative magneto-LC effects ($\bar{J} > 0$ and $\bar{J} < 0$) in the chiral and achiral N phases of **19**, respectively, with positive dielectric anisotropy ($\Delta\varepsilon > 0$), and (4) the proof of the existence of anisotropy in the intermolecular ferromagnetic interactions responsible for the positive magneto-LC effects by measuring the electric field dependence of molecular orientation and magnetic interactions in a surface-stabilized ferroelectric LC cell of **18** showing an chiral SmC* phase, by EPR spectroscopy. In this way, EPR spectroscopy turned out to be an excellent tool for analyzing the temperature dependence of the χ_{para} for organic nitroxide radical LC phases at high temperatures, for which SQUID magnetization measurement is not suited. Furthermore, it is of great advantage to be able to use EPR spectroscopy for evaluating the microscopic dynamic behavior of molecules and magnetic interactions (spin-spin interactions) in the nitroxide radical LC phases.

In the near future, the EPR techniques employed here would be applied to the characterization of novel metal-free magnetic soft materials, such as ionic liquid crystals, micelles, emulsions, and gels which will be developed on the basis of the nitroxide radical chemistry.

[a] Graduate School of Human and Environmental Studies, Kyoto University, Kyoto 606-8501, Japan. Fax:+81-75-753-7915; Tel:+81-75-753-6815; E-mail: tamura.rui.8c@kyoto-u.ac.jp; suzuki.katsuaki.45c@st.kyoto-u.ac.jp

[b] Graduate School of Engineering Science, Osaka University, Toyonaka, Osaka 560-8531, Japan. Fax:+81-6-6850-6256; Tel:+81-6-6850-6256; E-mail: yuchida@cheng.es.osaka-u.ac.jp

[c] Quantum Beam Science Directorate, Japan Atomic Energy Agency, Ibaraki 319-1195, Japan. Fax:+81-29-284-3511; Tel:+81-29-284-3834; E-mail: noda.yohei@jaea.go.jp

References

1. G. I. Likhtenshtein in *Nitroxides: Applications in Chemistry, Biochemistry and Materials Science*, ed. G. I. Likhtenshtein, J. Yamauchi, S. Nakatsuji, A. Smirnov and R. Tamura, Wiley-VCH, Weinheimn, 2008, p 205.
2. C. F. Polnaszek, J. H. Freed, *J. Phys. Chem.*, 1975, **79**, 2283.
3. J. S. Hwang, M. A. Morsy and G. A. Oweimreen, *J. Phys. Chem.*, 1994, **98**, 9056.
4. A. Nayeem, S. B. Rananavare, V. S. S. Sastry and J. H. Freed, *J. Chem. Phys.*, 1992, **96**, 3912.
5. D. Frezzato, G. Kothe and G. J. Moro, *J. Phys. Chem. B*, 2004, **108**, 9505.
6. K. Ohno and J. Sohma, *J. Magn. Reson.*, 1984, **58**, 1.
7. J. S. Hwang and G. A. Oweimreen, *Appl. Magn. Reson.*, 2004, **26**, 387.
8. D. Ionescu, G. R. Luckhurst and D. S. Desilva, *Liquid Crystals*, 1997, 23, 833

9. I. Dozov, N. Kirov and B. Petroff, *Phys. Rev. A*, 1987, **36**, 2870.

10. A. Nayeem and J. H. Freed, *J. Phys. Chem*., 1989, **93**, 6539.

11. S. Mita and S. Kondo, *Mol. Cryst. Liq. Cryst*., 1986, **140**, 153.

12. A. Nayeem, S. B. Rananavare, V. S. S. Sastry and J. H. Freed, *J. Chem. Phys*., 1989, **91**, 6887.

13. Y. Uchida, S. Oki, R. Tamura, T. Sakaguchi, K. Suzuki, K. Ishibashi and J. Yamauchi, *J. Mater. Chem*., 2009, **19**, 6877.

14. V. Strehmel, H. Rexhausen and P. Strauch, *Tetrahedron Lett*., 2010, **51**, 747.

15. M. Dvolatitzky, C. Taupin and F. Polydy, *Tetrahedron Lett*.,1976, **18**, 1469.

16. M. Dvolaitzky, J. Billard and F. Polydy, *C. R. Acad. Sci.,* 1974, **279C**, 533.

17. M. Dvolaitzky, J. Billard and F. Polydy, *Tetrahedron*, 1976, **32**, 1835.

18. S. Nakatsuji, M. Mizumoto, H. Ikemoto, H. Akutsu and J. Yamada, *Eur. J. Org. Chem*., 2002, 1912.

19. J. Allgaier and H. Finkelmann, *Macromol. Chem. Phys*., 1994, **195**, 1017.

20. S. Greve, V. Vill and W. Friedrichsen, *Z. Naturforsch*, 2002, **57b**, 677.

21. N. Ikuma, R. Tamura, S. Shimono, N. Kawame, O. Tamada, N. Sakai, J. Yamauchi and Y. Yamamoto, *Angew. Chem. Int. Ed*., 2004, **43**, 3677.

22. N. Ikuma, R. Tamura, S. Shimono, Y. Uchida, K. Masaki, J. Yamauchi, Y. Aoki and H. Nohira, *Adv. Mater*., 2006, **18**, 477.

23. N. Ikuma, R. Tamura, K. Masaki, Y. Uchida, S. Shimono, J. Yamauchi, Y. Aoki and H. Nohira. *Ferroelectrics*, 2006, **343**, 119.

24. R. Tamura, Y. Uchida and N. Ikuma, *J. Mater. Chem*., 2008, **18**, 2872. (Highlight)

25. N. A. Chumacova, A. Kh. Vorobiev, N. Ikuma, Y. Uchida, and R. Tamura, *Mendeleev Commun*., 2008, **18**, 21.

26. D. Kivelson, *J. Chem. Phys*., 1960, **33**, 1094.

27. Y. Noda, S. Shimono, M. Baba, J. Yamauchi, N. Ikuma amd R. Tamura, *J. Phys. Chem. B*, 2006, **110**, 23683.

28. Y. Uchida, R. Tamura, N. Ikuma, S. Shimono, J. Yamauchi, Y. Shimbo, H. Takezoe, Y. Aoki and H. Nohira, *J. Mater. Chem*., 2009, **19**, 415.

29. Y. Uchida, K. Suzuki, R. Tamura, N. Ikuma, S. Shimono, Y. Noda and J. Yamauchi, *J. Am. Chem. Soc*., 2010, **132**, 9746.

30. Y. Uchida, N. Ikuma, R. Tamura, S. Shimono, Y, Noda, J. Yamauchi, Y. Aoki, and H. Nohira, *J. Mater. Chem*., 2008, **18**, 2950-2952.

31. I. Haller, *Prog. Solid State Chem*., 1975, **10**, 103.

32. V. Manjuladevi and N. V. Mandhusadana, *Curr. Sci*., 2003, **85**, 1056.

33. Y. Noda, S. Shimono, M. Baba, J. Yamauchi, N. Ikuma and R. Tamura, *Appl. Magn. Reson*., 2008, **33**, 251.

34. K. Suzuki, Y. Uchida, R. Tamura, S. Shimono and J. Yamauchi, *J. Mater. Chem*., 2012, **22**, 6799.